Letter

Subgigahertz Multilayer-Graphene Nanoelectromechanical System Integrated with a Nanometer-Scale Silicon Transistor Driven by Reflectometry

Katsuhiko Nishiguchi,* Hiroshi Yamaguchi, and Akira Fujiwara
NTT Basic Research Laboratories, Nippon Telegraph and Telephone Corporation, 3-1 Morinosato Wakamiya, Atsugi, Kanagawa 243-0198, Japan

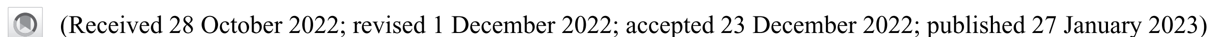
(Received 28 October 2022; revised 1 December 2022; accepted 23 December 2022; published 27 January 2023)

We demonstrate the detection of mechanical oscillations of a nanoelectromechanical system (NEMS) composed of a multilayer-graphene (MLG) membrane by using a Si field-effect transistor (FET). The MLG membrane of 500 nm in length is suspended above multiple nanowire channels of the FET functioning as a sensor with high sensitivity. A microwave probe in contact with the FET is connected to double-resonant circuits composed of two inductors and capacitors, and a radio-frequency (rf) signal drives the FET in the resonant condition. When the MLG membrane functioning as a gate of the FET oscillates in mechanical resonance and modulates impedance of the FET, this modulation is monitored using a reflected signal from the resonant circuits. By adjusting the resonant condition using a variable capacitor, the mechanical oscillations of the MLG membrane are detected at 340 MHz. Such rf-signal-driven readout of the NEMS operating at subgigahertz frequency will lead to highly sensitive and functional sensors for small mass and quantum mechanics as well as timing devices.

DOI: 10.1103/PhysRevApplied.19.L011003

A nanoelectromechanical system (NEMS) is a submicrometer-scale device having electrical and mechanical functionalities. Such a small structure enables a NEMS to oscillate mechanically at high frequency and thus to have fascinating functions such as high-sensitivity mass sensing [1–3] as well as platforms supporting study of quantum mechanics [4]. The mechanism of the NEMS mass sensors is based on that an object of small mass (Δm) to be detected changes the oscillation frequency f_{NEMS} of the NEMS. This frequency change Δf is proportional to $\Delta m f_{\mathrm{NEMS}}/M_{\mathrm{NEMS}}$, where M_{NEMS} is the mass of the oscillating NEMS membrane. Therefore, smaller M_{NEMS} is preferable for high-sensitivity mass sensors. Graphene [5] is a single-atomic-layer sheet of carbon and has unique mechanical properties such as high stiffness, high strength, and light weight [6–10]. These properties enable a graphene sheet to be used for NEMS sensors with high sensitivity [11,12]. Since graphene sheets also function as a charge sensor to detect the charge of one individual molecule [13], a combination of such charge sensing with mechanical mass sensing would enable a sensor to identify similar objects such as gas and molecules. Based on reports on carbon-nanotube-based mass sensors with atomic resolution, f_{NEMS} is needed to be several hundreds of megahertz or higher [1–3]. In addition to sensing applications, graphene NEMSs can be used as platforms for academic research on quantum mechanics such as nonlinear mechanics [14] and optomechanics [15]. Quantum harmonic oscillation or quantum ground state is also an exciting research field [4], in which a graphene NEMS may play an important role due to its high quality factor [14,15] and light weight. These research fields also need a NEMS to operate at several hundreds of megahertz or higher. However, readout of such high-frequency oscillations of a graphene NEMS is still difficult. One of the reasons for this difficulty is that such high oscillation frequency needs the length of the graphene membrane to be shortened to the submicrometer range. In order to read out submicrometer membranes, electrical readout is desirable because a membrane's length shorter than the wavelength of visible light makes use of optical readout, such as doppler interferometry, difficult. Electrical readout at several hundreds of megahertz or higher needs optimization of measurement systems, such as impedance matching. However, such optimization of a graphene sheet at high frequency is not straightforward because electrical and fabrication reproducibility of a graphene sheet is still challenging. Even for other NEMSs with membranes composed of other materials including silicon and silicon nitride, their oscillation signals at several hundreds of megahertz or higher are promising for functionalities such as high-frequency timing devices used for light detection and ranging, radar, and time of flight. However, such high-frequency readout is also difficult.

Here, using a high-sensitivity Si field-effect transistor (FET) having charge sensitivity with single-electron

*katsuhiko.nishiguchi.vu@hco.ntt.co.jp

 © 2023 American Physical Society

resolution, we demonstrate readout of mechanical oscillations of a NEMS. In order to demonstrate readout of high-frequency signals, the NEMS is composed not of monolayer graphene but of multilayer graphene (MLG) with a thickness of 3.5 nm. The MLG membrane above the FET's multiple channels functions as a FET gate. In order to read out membrane oscillations modulating the FET's impedance, the FET is connected to resonant circuits and driven by a radio-frequency (rf) signal in the resonant condition. Since readout at high frequency is optimized in the FET and resonant circuits, the MLG membrane can be formed separately from the electrical optimization. In addition, in order to ease this technique, so-called reflectometry [16,17], using the rf signal, a commercial microwave probe connected to resonant circuits mounted on a printed circuit board is used and put in contact with the FET.

Figure 1 shows the structure of the MLG NEMS integrated with the Si FET. The FET with multiple nanowire channels is fabricated from a silicon-on-insulator (SOI) wafer. Initial resistivity of the SOI layer and Si substrate is about 10 Ω cm. The thickness of the buried oxide layer is 400 nm. Ten nanowires and wider channels are patterned on the SOI layer, followed by oxidation at 1000 °C for 70 min. This oxidation forms a 40-nm-thick gate oxide and reduces the width and thickness of the nanowire channels to about 10 nm. The nanowire channel length is about 100 nm. Such a small channel enables the FET to detect single electrons even at room temperature [18]. The reason why multiple channels are used is explained below. Next, gate electrodes, hereafter referred to as dc gates, made of poly-Si are formed, followed by oxidation at 700 °C for 270 min and at 1000 °C for 8 min. The thicknesses of poly-Si and oxide are 80 and 40 nm, respectively. Next, phosphorus ions are heavily implanted, except for the nanowire channels, followed by thermal activation. Al contact pads of a ground-signal-ground pattern for a microwave probe are formed on the source and drain of the nanowire channels as signal and ground lines, respectively. Then, other gates (rf gates) made of 30-nm-thick Au on 3-nm-thick Ti are formed by a lift-off process. The gap between the two rf gates is 500 nm. Contact pads of the rf gates are also composed of a ground-signal-ground pattern for another microwave probe. Finally, a MLG sheet functioning as a membrane of the NEMS is suspended above the rf gates using a soft polymer film [19].

The MLG membrane suspended above the FET's channels functions as an oscillating gate for the FET. The impedance of the nanowire channels is modulated when a rf signal, $S_{\rm rf}$, applied to the rf gates oscillates the MLG membrane at the mechanical resonance frequency. The dc gates are used to induce an inversion layer in the Si channel under the dc gates. They also shield the FET channels under the dc gates from the electric field from the rf gates, which makes the Si channel under the dc gates highly conductive regardless of the rf gates. In addition, since the threshold voltage of the current-voltage characteristics originating from the nanowire channels is higher than that from the wider channel, current flowing through the FET is dominated by the impedance of the nanowire channels [20], which means that the area that dominates the FET's impedance is restricted to the multiple nanowire channels under the MLG membrane.

Figure 2 shows schematics of a reflectometry technique used for detecting mechanical oscillations of the MLG NEMS. A microwave probe is put in contact with the source of the FET, and the probe and contact pad of the FET constitute a stray capacitor, $C_{\rm stray}$ of 7.2 pF. The probe is connected to two inductors and a variable capacitor $C_{\rm var}$, all of which are mounted on a printed circuit board [Fig. 2(b)], and they function as double-resonant circuits connected to the FET as shown in Fig. 2(a). Its equivalent circuit is shown in Fig. 3(a). The double-resonant circuits connected to the FET have lower and higher resonance frequencies, $f_{\rm reso-L}$ and $f_{\rm reso-H}$, at which the reflection

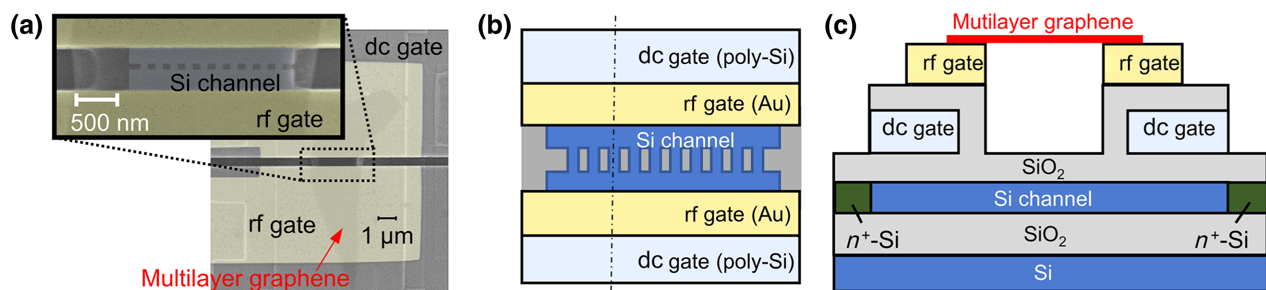

FIG. 1. (a) False-color scanning electron microscope image. The inset is an enlarged image of the area surrounded by the dotted line. The slightly shaded area is a MLG sheet whose thickness is about 3.5 nm. (b) Schematic of image in (a). For simplicity, the MLG sheet is not shown here. (c) Cross-sectional view along the dot-dashed line in (b). The drain and source are highly conductive due to n^+-Si and connected to aluminum electrodes. In (a), ten Si nanowire channels connected in parallel between two wider Si channels used for the drain and source are observed via the MLG sheet suspended between the two rf gates because the graphene sheet is thin enough for the electron beam to go through it.

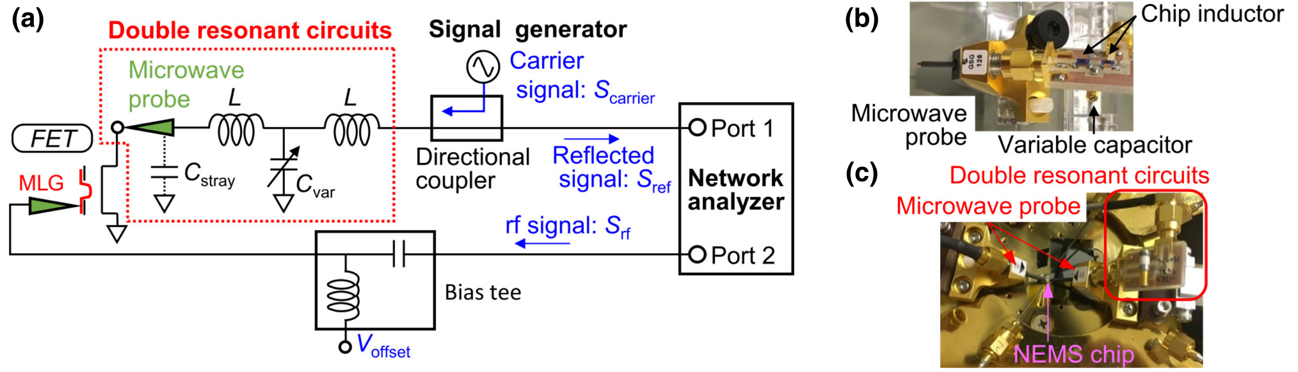

FIG. 2. (a) Schematics of a reflectometry technique for detecting mechanical oscillations of the MLG NEMS. (b) Photograph of the microwave probe connected to the double-resonant circuits mounted on a printed circuit board. (c) Photograph of the NEMS chip, microwave probes, and double-resonant circuits in a probe station. Stray capacitance C_{stray} originating from the microwave probe and contact pad of the FET is evaluated to be 7.2 pF. C_{var} is a variable capacitor (Johanson Manufacturing 5201). The inductance L is 100 nH (Coilcraft 1206CS). For simplicity, dc gates are not shown here because the electrical characteristics are dominated by a rf gate. A carrier signal whose frequency f_{carrier} is 140 MHz is supplied from a Keysight N5181B. The network analyzer is a Keysight E5080A. A rf signal whose frequency is f_{rf} is supplied from port 2, and offset bias, V_{offset}, is added at a bias tee. A reflected signal at a frequency of $f_{\mathrm{carrier}} + f_{\mathrm{rf}}$ is monitored at port 1 using the frequency offset function of the Keysight E5080A.

coefficient S_{11} characteristics show two dips [Fig. 3(c)]. A signal around the resonance frequencies can be transmitted in the circuit because its impedance around these frequencies is close to that for impedance matching. Otherwise, the signal is reflected from the circuit and thus cannot drive it. Therefore, a carrier signal S_{carrier} whose frequency f_{carrier} is close to $f_{\mathrm{reso-L}}$ is applied to the FET connected to the double-resonant circuits through a directional coupler. A signal S_{rf} with a frequency f_{rf} is added to dc offset voltage V_{offset} and applied to the rf gate connected to the MLG membrane functioning as the gate of the FET. S_{rf} modulates the FET's impedance and thus impedance-matching condition: when powers of S_{carrier} and S_{rf} are proportional to $\sin(2\pi t f_{\mathrm{carrier}})$ and $\sin(2\pi t f_{\mathrm{rf}} + \theta)$, respectively, the FET's impedance modulated by S_{rf} is proportional to $\sin(2\pi t f_{\mathrm{carrier}}) \times \sin(2\pi t f_{\mathrm{rf}} + \theta) = -[\cos\{2\pi t(f_{\mathrm{carrier}} + f_{\mathrm{rf}}) + \theta\} - \cos\{2\pi t(f_{\mathrm{carrier}} - f_{\mathrm{rf}}) - \theta\}]/2$, where θ is the difference of phase between S_{rf} and S_{carrier}, because the FET is driven in the linear region. This modulation corresponds to frequency mixing between f_{carrier} and f_{rf} and generates signals at $f_{\mathrm{carrier}} \pm f_{\mathrm{rf}}$ like in a frequency mixer. Then, since a frequency spectrum of a reflected signal S_{ref} has signals at f_{rf}, f_{carrier}, and $f_{\mathrm{carrier}} \pm f_{\mathrm{rf}}$ as shown in Fig. 3(b), monitoring S_{ref} at $f_{\mathrm{carrier}} + f_{\mathrm{rf}}$ corresponds to detection of S_{rf}. It should be noted that since $f_{\mathrm{carrier}} + f_{\mathrm{rf}}$ must be close to resonance frequencies for transmitting the signal in the resonant circuits, their multiple resonance frequencies play important roles in expanding a range of detectable signal frequency, which is a technical advance compared with conventional reflectometry techniques.

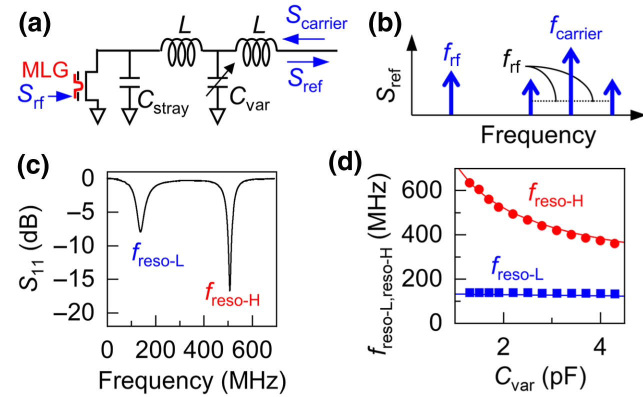

FIG. 3. (a) Equivalent circuit and (b) schematic frequency spectrum of a reflected signal in reflectometry. (c) Coefficient S_{11} characteristics of the double-resonant circuits connected to the FET. Higher and lower resonance frequencies, $f_{\mathrm{reso-H}}$ and $f_{\mathrm{reso-L}}$, are 140 and 513 MHz, respectively. S_{rf} applied to the MLG is grounded. (d) Change in $f_{\mathrm{reso-L}}$ and $f_{\mathrm{reso-H}}$ as a function of C_{var}. Filled symbols are experimental results. The solid lines are curves fitted to the experimental results with Eqs. (1) and (2) in the main text. C_{var} is evaluated from the resonance frequency of another resonant circuit composed of one inductor and C_{var}.

The closer $f_{\mathrm{carrier}} + f_{\mathrm{rf}}$ is to $f_{\mathrm{reso-H}}$, the greater is the signal amplitude of S_{ref}, which means that S_{rf} can be detected with higher sensitivity. Therefore, we adjust $f_{\mathrm{reso-L}}$ and $f_{\mathrm{reso-H}}$ by changing C_{var} so that the sensitivity would be good at the mechanical resonance frequency f_{graphene} of the MLG NEMS. $f_{\mathrm{reso-L}}$ and $f_{\mathrm{reso-H}}$ are given roughly by the following simplified equations:

$$f_{\mathrm{reso\text{-}L}} = \frac{1}{2\pi}\sqrt{\frac{2C_{\mathrm{stray}} + C_{\mathrm{var}} - \sqrt{4{C_{\mathrm{stray}}}^2 + {C_{\mathrm{var}}}^2}}{2LC_{\mathrm{stray}}C_{\mathrm{var}}}}, \quad (1)$$

$$f_{\text{reso - H}} = \frac{1}{2\pi}\sqrt{\frac{2C_{\text{stray}} + C_{\text{var}} + \sqrt{4C_{\text{stray}}^{\ 2} + C_{\text{var}}^{\ 2}}}{2LC_{\text{stray}}C_{\text{var}}}}. \quad (2)$$

As shown in Fig. 3(d), these equations can trace the experimental results obtained when the resonance frequencies are tuned by C_{var}. $f_{\text{ graphene}}$ is estimated mathematically as

$$f_{\text{graphene}} = \sqrt{\left(A\sqrt{\frac{E}{\rho}}\frac{t}{L^2}\right)^2 + \frac{0.57\ TA^2}{\rho L^2 wt}}, \quad (3)$$

where E (1 TPa) is Young's modulus, ρ (2200 kg/m^3) is the mass density, T is tension, A (1.03) is the clamping coefficient, and t (3.5 nm), w, and L (500 nm) are the thickness, width, and length of the graphene [11]. When T is zero, $f_{\text{ graphene}}$ is estimated to be 307 MHz. Then, according to these estimations, the charge-sensitivity characteristics are modulated by C_{var}.

In this work, by using the S_{12} analysis of a vector network analyzer (VNA), frequency $f_{\text{ rf}}$ of S_{rf} output from port 2 of the VNA is swept, and the ratio $S_{\text{ref/rf}}$ ($= S_{\text{ref}}/S_{\text{rf}}$) of S_{rf}, input to port 1 of the VNA, at $f_{\text{ carrier}} + f_{\text{ rf}}$ is monitored as a signal originating from the MLG using the frequency offset function of the VNA. Figure 4(a) shows the change in $S_{\text{ref/rf}}$ as a function of $f_{\text{ rf}}$ at atmospheric pressure as reference characteristics. There is a large peak, depicted by a broken line as a guide, around 370 MHz. This frequency is close to $f_{\text{ reso−H}} - f_{\text{ carrier}}$, which means that since the sensitivity of the FET driven by reflectometry is good around $f_{\text{ reso−H}} - f_{\text{ carrier}}$, $S_{\text{ref/rf}}$ becomes large around this frequency even when the MLG membrane does not oscillate. Therefore, the appearance of this large peak means that the reflectometry works exactly as it is supposed to. On the other hand, there are other small peaks, e.g., at 355, 368, 374, and 386 MHz. They are likely to originate from unintentional characteristics of the device because of its complicated structure, such as two-layer gates having a gap, as explained below. Therefore, these peaks can be identified as a background signal.

Figure 4(b) shows $f_{\text{ rf}}$ dependence of $S_{\text{ref/rf}}$ at vacuum and atmospheric pressures. In characteristics at both pressures, $S_{\text{ref/rf}}$ increases with $f_{\text{ rf}}$ as a background signal. At vacuum pressure, one peak appears around 340 MHz. By subtracting $S_{\text{ref/rf}}$–$f_{\text{ rf}}$ characteristics at atmospheric pressure from those at vacuum pressure, this additional peak can be fitted by a Lorentzian curve as shown in Fig. 4(c). These features suggest that the peak at around 340 MHz originates from mechanical oscillations of the MLG membrane functioning as the oscillating gate of the FET and that the oscillations are damped at atmospheric pressure. Additionally, when the offset dc voltage V_{offset} superimposed on the rf signal is changed from 0 to 3 V, the frequency of the additional peak increases, as indicated by the

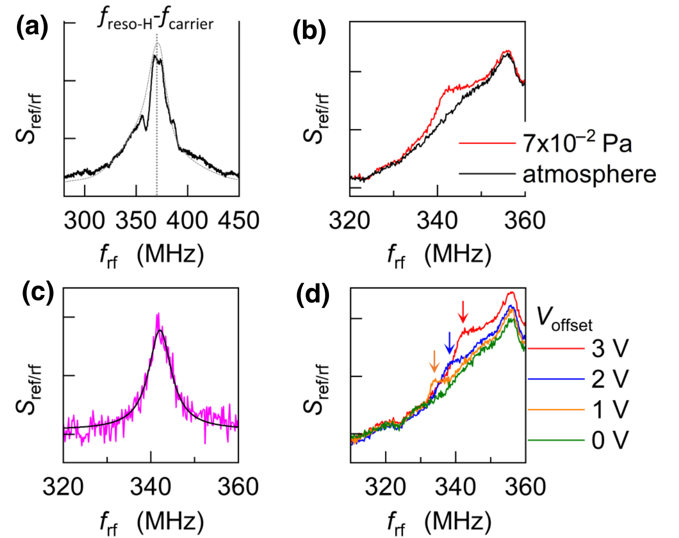

FIG. 4. (a) Change in the ratio $S_{\text{ref/rf}}$ of S_{ref} to S_{rf} when frequency $f_{\text{ rf}}$ is changed at atmospheric pressure. V_{offset} is 0 V. Powers of S_{carrier} and S_{rf} are 10 and 5 dBm, respectively. The dotted line indicates the frequency given by $f_{\text{ reso−H}} - f_{\text{ carrier}}$ ($= 373$ MHz). The broken line is a guide to the eye and represents a large peak described in the main text. (b) $f_{\text{ rf}}$ dependences of $S_{\text{ref/rf}}$ at 7×10^{-2} Pa and atmospheric pressure. Power and offset dc voltage, V_{offset}, of the rf signal are 5 dBm and 3 V, respectively. (c) Difference in $S_{\text{ref/rf}}$ characteristics at 7×10^{-2} Pa and atmospheric pressure shown in (b). The solid line is the Lorentzian curve fitted to the difference in $S_{\text{ref/rf}}$ characteristics. The quality factor estimated from the Lorentzian curve is 57. (d) $S_{\text{ref/rf}}$ characteristics when V_{offset} is changed. The arrows indicating the additional peaks are also shown as a guide.

arrows shown in Fig. 4(d). The likely reason for this shift is that the tension in the graphene sheet increases with V_{offset} [9]. On the other hand, other peaks at around 355 MHz are independent of pressure. Although $S_{\text{ref/rf}}$ increases slightly with V_{offset} due to a change in the impedance of the FET channel by V_{offset}, frequencies of these peaks at 355 MHz are constant. Other devices also show small dips and peaks in S_{11} and $S_{\text{ref/rf}}$ characteristics, respectively, near resonance frequencies. These features of the peaks at 355 MHz mean that they originate not from the graphene oscillation but from the unintentional characteristics of the device because of its complicated structure.

Finally, we discuss how to improve sensitivity to detect NEMS oscillations. In this work, we use multiple channels of FETs. In reflectometry, sensitivity can be improved by adjusting the impedance of the FET connected to the double-resonant circuits so as to be equal to the characteristic impedance, 50 Ω, for impedance matching. Since the impedance of the single channel of the FET is too high to achieve this impedance matching, multiple channels are used in order to reduce the impedance. However, since the impedance is still higher than that for perfect impedance matching, optimization of the FET and

double-resonant circuits leads to further improvement of sensitivity. Another way to improve sensitivity is reduction in C_{stray}. This time, while we use the microwave probe in order to ease the reflectometry, use of the probe leads to larger stray capacitance. Since a smaller capacitance improves the sensitivity of the FET, an integration of the FET with the resonant circuits is one way to improve sensitivity. Since improvement of sensitivity leads to detection of NEMS oscillations at higher frequency, our technique using reflectometry with the double-resonant circuits holds promise for functioning as a high-sensitivity mass sensor.

In conclusion, we demonstrate detection of mechanical oscillations of a MLG NEMS using a multichannel FET. In order to detect the MLG membrane oscillating at a few hundreds of megahertz, we use reflectometry in which double-resonant circuits are connected to a microwave probe in contact with the NEMS. Since reflectometry can be used to detect change in capacitance, such reflectometry can be available for expanding detectable frequency of other NEMSs in which the signal originates from capacitance modulation. Such high versatility of reflectometry will lead to higher performance not only in graphene NEMSs, but also in other mechanical resonators, e.g., for sensors and timing devices.

Acknowledgments.—We are grateful to G. A. Steele and H. S. J. van der Zant of Delft University of Technology for valuable discussions.

[1] H.-Y. Chiu, P. Hung, H. M. C. Postma, and M. Bockrath, Atomic-scale mass sensing using carbon nanotube resonators, Nano Lett. **8**, 4342 (2008).

[2] K. Jensenb, K. Kim, and A. Zettle, An atomic-resolution nanomechanical mass sensor, Nat. Nanotech. **3**, 533 (2008).

[3] J. Chaste, A. Eichler, J. Moser, G. Ceballos, R. Rurali, and A. Bachtold, A nanomechanical mass sensor with yoctogram resolution, Nat. Nanotech. **7**, 301 (2012).

[4] A. D. O'Connell, M. Hofheinz, M. Ansmann, R. C. Bialczak, M. Lenander, L. Lucero, M. Neeley, D. Sank, H. Wang, M. Weides, *et al.*, Quantum ground state and single-phonon control of a mechanical resonator, Nature **464**, 697 (2010).

[5] A. K. Geim and K. S. Novoselov, The rise of graphene, Nat. Mater. **6**, 183 (2007).

[6] C. Lee, X. Wei, J. W. Kysar, and J. Hone, Measurement of the elastic properties and intrinsic strength of monolayer graphene, Science **321**, 385 (2008).

[7] D. Garcia-Sanchez, A. M. van der Zande, A. S. Paulo, B. Lassagne, P. L. McEuen, and A. Bachtold, Imaging mechanical vibrations in suspended graphene sheets, Nano Lett. **8**, 1399 (2008).

[8] J. S. Bunch, S. S. Verbridge, J. S. Alden, A. M. van der Zande, J. M. Parpia, H. G. Craighead, and P. L. McEuen, Impermeable atomic membranes from graphene sheets, Nano Lett. **8**, 2458 (2008).

[9] C. Chen, S. Lee, V. V. Deshpande, G. H. Lee, M. Lekas, K. Shepard, P. Kim, and J. Hone, Graphene mechanical oscillators with tunable frequency, Nat. Nanotech. **8**, 923 (2013).

[10] C. Chen and J. Hone, Graphene nanoelectromechanical systems, Proc. IEEE **101**, 1766 (2013).

[11] J. S. Bunch, A. M. van der Zande, S. S. Verbridge, I. W. Frank, D. M. Tanenbaum, J. M. Parpia, Harold G. Craighead, and P. L. McEuen, Electromechanical resonators from graphene sheets, Science **315**, 490 (2007).

[12] A. Y. Zhu, F. Yi, J. C. Reed, H. Zhu, and E. Cubukcu, Optoelectromechanical multimodal biosensor with graphene active region, Nano Lett. **14**, 5641 (2014).

[13] J. Sun, M. Muruganathan, and H. Mizuta, Room temperature detection of individual molecular physisorption using suspended bilayer graphene, Sci. Adv. **2**, e1501518 (2016).

[14] A. Eichler, J. Moser, J. Chaste, M. Zdrojek, I. Wilson-Rae, and A. Bachtold, Nonlinear damping in mechanical resonators made from carbon nanotubes and graphene, Nat. Nanotech. **6**, 339 (2011).

[15] V. Singh, S. J. Bosman, B. H. Schneider, Y. M. Blander, A. Castellanos-Gomez, and G. A. Steele, Optomechanical coupling between a multilayer graphene mechanical resonator and a superconducting microwave cavity, Nat. Commun. **9**, 820 (2014).

[16] R. J. Schoelkopf, P. Wahlgren, A. A. Kozhevnikov, P. Delsing, and D. E. Prober, The radio-frequency single-electron transistor (RF-SET): A fast and ultrasensitive electrometer, Science **280**, 1238 (1998).

[17] K. Nishiguchi, H. Yamaguchi, A. Fujiwara, H. S. J. Zant, and G. A. Steele, Wide-bandwidth charge sensitivity with a radio-frequency field-effect transistor, Appl. Phys. Lett. **103**, 143102 (2013).

[18] K. Nishiguchi, C. Koechlin, Y. Ono, A. Fujiwara, H. Inokawa, and H. Yamaguchi, Single-electron-resolution electrometer based on field-effect transistor, Jpn. J. Appl. Phys. **47**, 8305 (2008).

[19] A. Castellanos-Gomez, M. Buscema, R. Molenaar, V. Singh, L. Janssen, H. S. J. van der Zant, and G. A. Steele, Deterministic transfer of two-dimensional materials by all-dry viscoelastic stamping, 2D Mater. **1**, 011002 (2014).

[20] A. Fujiwara, S. Horiguchi, M. Nagase, and Y. Takahashi, Threshold voltage of Si single-electron transistor, Jpn. J. Appl. Phys. **42**, 2429 (2003).